Cancer Research

Interleukin-30/IL27p28 Shapes Prostate Cancer Stem-like Cell Behavior and Is Critical for Tumor Onset and Metastasization

Carlo Sorrentino[1,2,3], Stefania L. Ciummo[1,2,3], Giuseppe Cipollone[4,5], Sara Caputo[6], Matteo Bellone[6], and Emma Di Carlo[1,2,3]

Abstract

Prostate cancer stem-like cells (PCSLC) are believed to be responsible for prostate cancer onset and metastasis. Autocrine and microenvironmental signals dictate PCSLC behavior and patient outcome. In prostate cancer patients, IL30/IL27p28 has been linked with tumor progression, but the mechanisms underlying this link remain mostly elusive. Here, we asked whether IL30 may favor prostate cancer progression by conditioning PCSLCs and assessed the value of blocking IL30 to suppress tumor growth. IL30 was produced by PCSLCs in human and murine prostatic intraepithelial neoplasia and displayed significant autocrine and paracrine effects. PCSLC-derived IL30 supported PCSLC viability, self-renewal and tumorigenicity, expression of inflammatory mediators and growth factors, tumor immune evasion, and regulated chemokine and chemokine receptor genes, primarily via STAT1/STAT3 signaling. IL30 overproduction by PCSLCs promoted tumor onset and development associated with increased proliferation, vascularization, and myeloid cell recruitment. Furthermore, it promoted PCSLC dissemination to lymph nodes and bone marrow by upregulating the CXCR5/CXCL13 axis, and drove metastasis to lungs through the CXCR4/CXCL12 axis. These mechanisms were drastically hindered by IL30 knockdown or knockout in PCSLCs. Collectively, these results mark IL30 as a key driver of PCSLC behavior. Targeting IL30 signaling may be a potential therapeutic strategy against prostate cancer progression and recurrence.

Significance: IL30 plays an important role in regulating prostate cancer stem-like cell behavior and metastatic potential, therefore targeting this cytokine could hamper prostate cancer progression or recurrence. *Cancer Res; 78(10); 2654–68. ©2018 AACR.*

Introduction

Prostate cancer is the most common male malignancy and the second leading cause of male cancer-related deaths in Europe and the United States (1). Mortality for prostate cancer is related to metastatic disease, which may develop in patients who become resistant to medical prostate cancer treatments, but it may also manifest many years after a radical, and apparently successful, surgical cure of a localized prostate cancer.

The immortal and pluripotent cancer-initiating cells, referred to as prostate cancer stem-like cells (PCSLC), which possess self-renewal capability and sustain the long-term clonal maintenance of the tumor, are believed to be responsible for treatment resistance, disease recurrence and metastasis (2). In their niche microenvironment, PCSLCs' entry and exit in dormancy is regulated by mostly unidentified autocrine and paracrine signals influencing the tumor microenvironment (TME; ref. 3), which, in turn, conditions cancer phenotype and clinical outcome (4).

So far, it has been shown that properties of PCSLCs may be regulated by matricellular glycoproteins, such as osteonectin (5); attachment factors, such as Annexin II/Annexin II receptor axis (6); hypoxia, through hypoxia-inducible factor generation (7); growth and angiogenic factors, such as VEGF/neuropilin 2 (8); osteogenic proteins, such as BMP7 (9) and chemoattractants, in particular, CXCL12 (10). Decoding the major autocrine and paracrine loops responsible for PCSLC's cycle reactivation and mobilization could provide tools for planning effective strategies against prostate cancer progression or recurrence.

We have recently reported that endogenous IL30, originally identified as IL27p28 subunit, a novel polypeptide related to IL12p35 (11), is expressed in prostate cancer by both cancer cells and cancer- or lymph node (LN)–infiltrating leukocytes and that it displays tumor-promoting functions. Indeed, in prostate cancer patients, its expression is tightly linked with advanced grade and stage of the disease (12, 13). The current view that the TME can impact a cell's stemness properties and thereby shape tumor progression and therapeutic response, raises the question whether the role of IL30 in prostate cancer biology is concealed in its effect on PCSLC behavior (4). This possibility has been widely explored in the present work.

[1]Division of Anatomic Pathology, "SS Annunziata" Hospital, Chieti, Italy. [2]Ce.S.I.-Me.T, Aging Research Center, Anatomic Pathology and Immuno-Oncology Unit, "G. d'Annunzio" University of Chieti-Pescara, Chieti, Italy. [3]Department of Medicine and Sciences of Aging, Division of Anatomic Pathology and Molecular Medicine, "G. d'Annunzio" University of Chieti-Pescara, Chieti, Italy. [4]General and Thoracic Surgery, "SS Annunziata" Hospital, Chieti, Italy. [5]Department of Medical, Oral and Biotechnological Sciences, "G. d'Annunzio" University of Chieti-Pescara, Chieti, Italy. [6]Cellular Immunology Unit, San Raffaele Scientific Institute, Milan, Italy.

Note: Supplementary data for this article are available at Cancer Research Online (http://cancerres.aacrjournals.org/).

C. Sorrentino and S.L. Ciummo contributed equally to this article.

Corresponding Author: Emma Di Carlo, Ce.S.I.-Me.T., Anatomic Pathology and Immuno-Oncology Unit, Via Luigi Polacchi 11, 66100, Chieti, Italy. Phone: 39-0871-541540; E-mail: edicarlo@unich.it

doi: 10.1158/0008-5472.CAN-17-3117

Materials and Methods

Cell cultures, flow cytometry, and MTT assay

Prostatic intraepithelial neoplasia-derived stem-like cells (PIN-SC) were provided by Dr. Matteo Bellone (San Raffaele Scientific Institute, Milan, Italy), who generated these cells from tumors developed in transgenic adenocarcinoma mouse prostate (TRAMP) model and characterized them in Mazzoleni and colleagues (14). The cell lines were authenticated by means of cell surface staining and flow cytometry for characteristic markers, and by their growth properties as described in ref. 14. PIN-SCs were cultured in ultralow attachment flasks (Corning), at 37°C in a humidified incubator, using serum-free medium (SFM), which consisted of DMEM:F12 (1:1), GlutaMAX-I supplement (Invitrogen), 50 ng/mL heparin (Sigma-Aldrich), 20 ng/mL EGF, and 10 ng/mL βFGF (R&D Systems), as described in ref. 14. Cells were cultured for less than 10 passages after thawing and occasionally tested for *Mycoplasma* contamination, using the MycoAlert PLUS *Mycoplasma* Detection Kit (Lonza), before experiments were performed (last tested in 2016). Recombinant (r) murine (m) IL30 (#7430-ML) was purchased from R&D Systems. IL30 receptor (R) expression in PIN-SCs was assessed by flow cytometry, and their proliferation by MTT, as described in the Supplementary Methods.

Transfection with *IL30* expressing vector

Engineering of the *IL30* lentiviral expression vector and its transfection into PIN-SCs, were performed as described in the Supplementary Methods.

IL30 silencing

Long-term silencing of *IL30* in PIN-SC cells was achieved by using short hairpin (sh) RNA Hush GFP-tagged lentiviral vectors from Origene (sequences are provided in the Supplementary Table S1), a gene-specific kit of four independent shRNA constructs in lentiviral GFP vector, designed to target *mIL30* gene. Noneffective scrambled shRNA was used as a control and the downregulation of *IL30* expression was confirmed by real-time RT-PCR, Western blot and ELISA. The four shRNAs, which showed a knockdown efficiency of 71%, 79%, 82%, and 89%, induced similar changes in proliferation rates, sphere-forming potential and gene expression profiles. Thus, we selected the constructs with the highest knockdown efficiency (89% and 82%) for subsequent *in vivo* experiments. The infected cells were sorted using a FACSAria II Cell Sorter and GFP as marker.

CRISPR/Cas9-mediated *IL30* gene knockout

To generate *IL30* knockout ($IL30^{-/-}$) PIN-SCs, we used CRISPR/Cas9 technology, as described in the Supplementary Methods (sequences of the two guideRNA used for CRISPR/Cas9-mediated *IL30* gene knockout are provided in the Supplementary Table S2). IL30 knockout was validated by Western blot and ELISA assay.

ELISA

The quantitation of Epstein-Barr virus–induced gene 3 (EBI3, also known as IL27 subunit beta), IL27, and IL27p28/IL30 proteins in the supernatant (sup) derived from (wild type and transfected) PIN-SCs, was assessed using the Mouse EBI3 ELISA Kit (LifeSpan BioSciences Inc.; detection sensitivity, 5.79 pg/mL), the LEGEND MAX Mouse IL27 Heterodimer (BioLegend; detection sensitivity, 16.9 pg/mL) and mIL27p28/IL30 Quantikine ELISA kit (R&D Systems; detection sensitivity, 4.27 pg/mL), respectively, according to the manufacturer's instructions.

Stat1 and *Stat3* knockdown experiments

Silencing of *Stat1* and *Stat3*, in PIN-SCs, was performed using the FlexiTube GeneSolution (Qiagen). Two siRNAs, for each transcription factor, with the highest knockdown efficiency, were selected, as reported in the Supplementary Methods.

Western blotting

Western blotting was performed to assess EBI3 expression in wild type PIN-SCs and IL30 expression in wild type PIN-SCs, IL30PIN-SCs, IL30shPIN-SCs, $IL30^{-/-}$PIN-SCs (and control clones), and to assess STAT1 or STAT3 expression in PIN-SCs transfected with siRNAs targeting *Stat1* or *Stat3*, as described in the Supplementary Methods.

Sphere formation and colony formation assays

Sphere formation assay (by using the Extreme Limiting Dilution Analysis, ELDA; ref. 15) and soft agar assay were performed as described in the Supplementary Methods.

Real-time RT-PCR and PCR arrays were performed as described in the Supplementary Methods.

Chemotaxis and migration assay

To assess the migration capacity of IL30-treated PIN-SCs toward CXCL12 or CXCL13, we used the QCM 3-μm Chemotaxis Assay 24-well-Colorimetric kit (Millipore), according to the manufacturer's instructions.

Mouse studies

Prostatic tissues from B6 TRAMP mice (The Jackson Laboratory) were used for immunoistochemical analyses. Normal prostate tissue was obtained from 9 weeks, PIN from 11 weeks, and adenocarcinoma from 28-weeks-old B6 TRAMP mice. Normal prostates from 9-weeks-old C57BL/6J mice (Envigo) were used as control. The tumorigenicity of PIN-SCs, was assessed by limiting dilution analysis by injecting subcutaneously or orthotopically, in C57BL/6J mice, a cell range from 2×10^6 to 1×10 cells per animal (20 mice per group).

Histopathology, immunohistochemistry, and TUNEL staining

Histology, immunohistochemistry, and TUNEL staining were performed as described in the Supplementary Methods, using the antibodies (Ab) listed in the Supplementary Table S3. Double immunostainings were performed as reported (13, 16). Proliferation index, microvessel and cell counts were assessed as described in the Supplementary Methods.

Statistical analysis

For *in vitro* and *in vivo* studies, between-group differences were assessed by Student *t* test or ANOVA with Tukey HSD test. Between groups differences in sphere-forming potential were evaluated by ELDA (15). All statistical tests were evaluated at an α level of 0.05, using Stata version 13 (Stata Corp).

Ethics committee approval

For study on human prostate samples, written informed consent was obtained from patients. The study was performed in

accordance with the principles outlined in the Declaration of Helsinki and approved by the ethical committee of the "G. d'Annunzio" University (PROT 1945/09 COET of July 14, 2009). All animal procedures were performed in accordance with institutional and European Community guidelines for animal experiments, and approved by the Institutional Animal Care Committee of "G. d'Annunzio" University (CEISA) and the Italian Ministry of Health (Authorization n. 399/2015-PR).

Results

PCSLCs release and respond to IL30, which increases their viability and self-renewal ability

Murine PCSLCs were isolated, and characterized by Mazzoleni and colleagues (14), from PIN that spontaneously developed in 11-week-old TRAMP mice (14), hemizygous for the rat probasin (*Pb*)-SV40gp6 large T antigen (*Tag*) transgene in a C57BL/6J background (17), a model of prostate cancer (18) that recapitulates the human disease (17). These cells, hereinafter referred to as PIN-SCs, showed a Sca-1^+/$CD133^+$/$CD44^{hi}$/$\alpha2\beta1^{hi}$/CD49f phenotype (19) and lacked androgen receptor and synaptophysin (14). PIN-SCs showed endless self-renewal ability, multilineage differentiation, tumorigenic potential, PCSLC-specific molecular signature (14) and expressed prostate cancer–associated antigens, but did not express Tag (19). When injected in nude mice, PIN-SCs reproduce, to some extent, the spontaneous tumor of origin (14).

To assess whether PIN-SCs might respond to IL30 stimulation, we first investigated the expression of what is currently known to be the IL30 receptor (R; ref. 20). PIN-SCs express both IL30R chains, gp130 (CD130; 99.9%) and IL6Rα (CD126; 9.5%; Fig. 1A), and constitutively express and release IL30 (182.82 pg/mL; Fig. 1B–D), whereas they do not produce and release neither EBI3, nor IL27 heterodimer, as assessed by Western blot and ELISA assay (Supplementary Fig. S1). The normal prostatic epithelium, from both B6 TRAMP and C57BL/6J mice, was negative for IL30 immunostaining, whereas PIN (21), from which PIN-SCs originate, was negative, except for Sca-1^+ cells found in the basal cell layer (Fig. 1E). The poorly differentiated carcinoma from TRAMP mice, which develops between 25 and 30 weeks of age (18), revealed a moderate to strong IL30 expression (Fig. 1E). Both PIN and poorly differentiated tumors expressed the two IL30R chains (Fig. 1F), which were also found in human PIN and prostate cancer (Supplementary Fig. S2).

In humans, IL30 was also absent in the normal prostatic glands, whereas it was expressed by rare $CD133^+$ stem-like cells located in the basal layer of PIN and in most of high-grade and stage prostate cancers (Fig. 1G), as previously observed (13).

To assess whether IL30 may serve as a growth factor for PIN-SCs, we analyzed their proliferation in response to rIL30 (2–200 ng/mL). IL30 significantly ($P < 0.01$) increased PIN-SC proliferation starting from 2 ng/mL and reaching a maximum at 50 ng/mL (Fig. 2A), whereas it was consistently ($P < 0.05$) hampered by the addition of anti–IL30Abs (Fig. 2B). Assessment of PIN-SCs' viability, after lentivirus(LV)-mediated transduction of *IL30* gene (IL30PIN-SCs) and after shRNA silencing of *IL30* gene (IL30shPIN-SCs. Clones D and B are represented), which respectively, increased or suppressed production of the cytokine, corroborated these data and also revealed that small changes (an increase of ∼2.24 ng/mL or a decrease of ∼0.176 ng/mL, respectively) in the amount of the cytokine released by tumor cells determined significant biological effects (Fig. 2B). In fact, proliferation was consistently ($P < 0.01$) increased in the former clone, whereas it was dramatically decreased in these last two clones, when compared with controls, namely empty−vector (EV)-*IL30* gene–transfected PIN-SCs (EV-IL30PIN-SCs), scrambled shRNA-transduced PIN-SCs (EV-IL30shPIN-SCs) and wild type PIN-SCs (Fig. 2B). The knockout of IL30 in PIN-SCs ($IL30^{-/-}$PIN-SCs) with CRISPR/Cas9-based approach (Supplementary Fig. S3) confirmed the autocrine function of the cytokine causing a substantial reduction in their proliferation (Fig. 2B).

PIN-SC's ability to form colonies and generate new spheres was significantly increased by rIL30 (20–100 ng/mL), starting from 50 ng/mL ($P < 0.0001$), when compared with controls (Fig. 2C–E). Clonogenic and sphere formation capabilities of PIN-SCs were significantly reduced by anti-IL30Abs ($P < 0.001$) and by IL30-knockdown in IL30shPIN-SCs ($P < 0.01$) or IL30 knockout in $IL30^{-/-}$PIN-SCs ($P < 0.01$), when compared with controls. Moreover, the number of both newly formed colonies and spheres was greatly increased in IL30PIN-SCs ($P < 0.01$), when compared with controls. Notably, the addition of anti–IL30Abs to the culture medium of IL30PIN-SCs abolished this response and inhibited their colony and sphere formation capabilities ($P < 0.01$; Fig. 2C and F).

IL30 boosts the tumorigenicity of PCSLCs, whereas its silencing prevents or delays tumor onset and progression

The effect of IL30 on the self-renewal ability of PIN-SCs was, then, tested in congenic, immune-competent C57BL/6J mice, to investigate the tumor–host relationship. The tumorigenicity of PIN-SCs was first tested, by limiting dilution analysis, with subcutaneous cell injections (Table 1). The lowest number of PIN-SCs capable of generating a subcutaneous tumor in, at least, 20% of mice was 2×10^4. When orthotopically injected, the same number of cells resulted in 50% of tumor take, whereas the lowest number of cells able to generate a tumor decreased to 1×10, with 5% of tumor take. IL30 overproduction, by IL30PIN-SCs, increased the tumor take and reduced the latency time, at all tested cell concentrations (Table 1).

Immunohistochemical analyses of orthotopic IL30PIN-SC tumors revealed that, in comparison with the IL30PIN-SC tumors developed after subcutaneous implantation of the same number of cells (2×10^4), their $Sca1^+$/$IL30^+$ cancer cell content was significantly higher (86.5 ± 10.2% vs. 64.0 ± 11.3%, Student *t* test, $P < 0.05$; Fig. 2G). Sca-1^+ cells were much more represented in orthotopic versus subcutaneously untransfected (68.0% ± 7.0% vs. 45.0% ± 6.1%, $P < 0.05$), or wild-type PIN-SC tumors (Fig. 2H), although their number significantly decreased when compared with orthotopically developed IL30PIN-SC tumors ($P < 0.05$; Fig. 2G; Supplementary Fig. S4). Cell counts were assessed by light microscopy on immunostained sections, with Qwin image analysis software, as described in the Supplementary Methods. The orthotopic implantation may thus select for stem-like cell phenotype and self-renewal capability, whereas IL30 promotes stemness whatever the site of tumor growth is.

Next, to assess whether, in the TME, IL30, by binding EBI3, may function as IL27 (20), we evaluated EBI3 expression in both subcutaneous and orthotopic PIN-SC tumors, and found it was undetectable (Supplementary Fig. S5).

The tumorigenicity of PIN-SCs was finally assessed in the presence of both IL30 overproduction, using IL30PIN-SCs, and IL30 silencing, using IL30shPIN-SCs, to mimic *in vivo* the

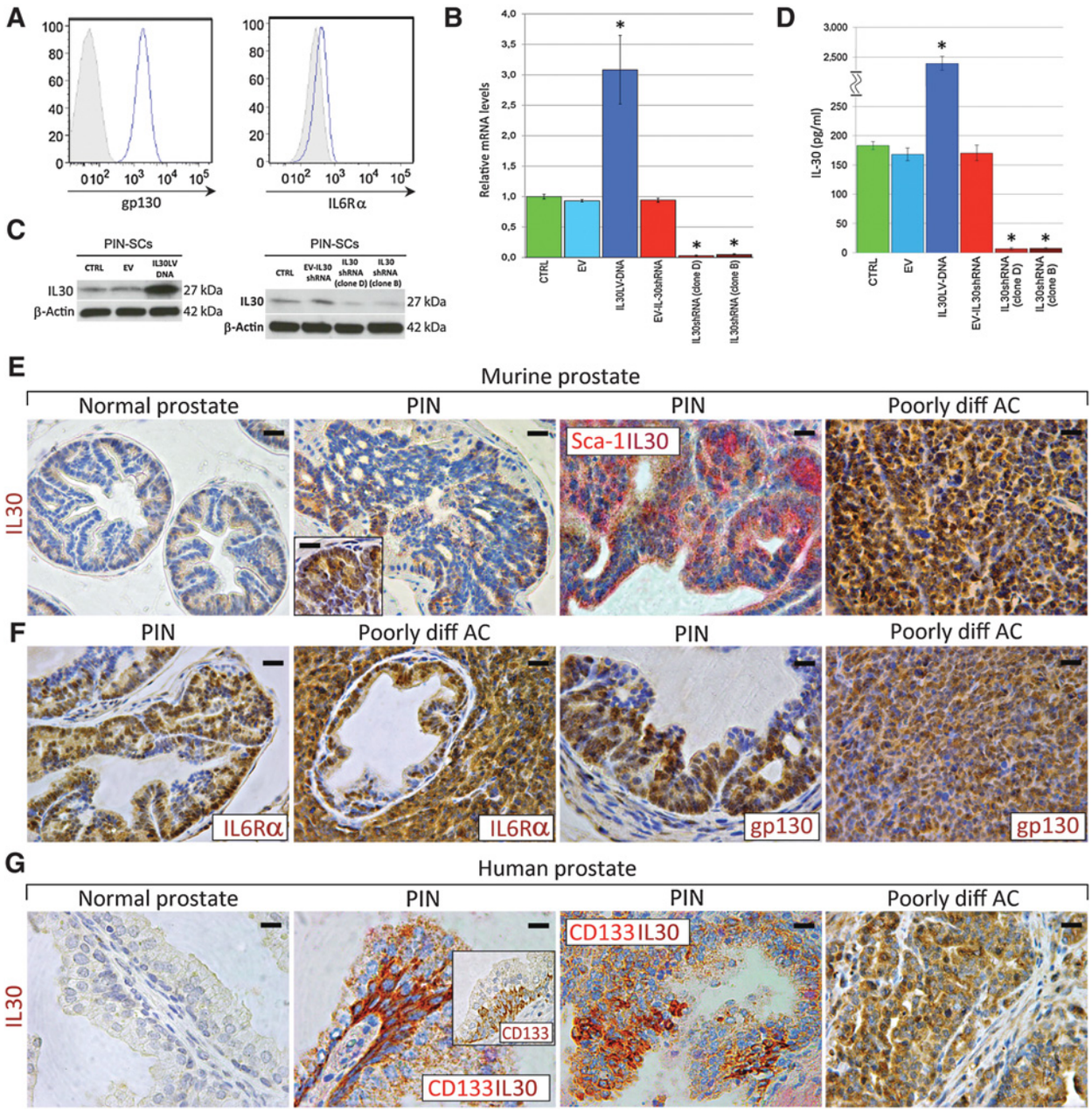

Figure 1.

Expression of IL30 and IL30R by PCSLCs, murine, and human prostate tissues. **A,** Cytofluorimetric analyses of gp130-(CD130) and IL6Rα- (CD126) expression in PIN-SCs. **B,** Relative expression ± SD of IL30 mRNA. CTRL, PIN-SCs. ANOVA, $P < 0.0001$. *, $P < 0.01$, Tukey HSD test compared with CTRL, EV, or EV-IL30shRNA (clones D and B). **C,** Western blot analyses of IL30 protein expression. **D,** ELISA assay of IL30 release by CTRL (182.82 ± 6.9 pg/mL), EV-PIN-SCs (168.21 ± 10.82 pg/mL), IL30PIN-SCs (2424.46 ± 83.9 pg/mL), EV-IL30shPIN-SCs (170.44 ± 13.09 pg/mL), and IL30shPIN-SCs (clone D, 6.76 ± 1.87 pg/mL; clone B, 7.53 ± 1.38 pg/mL). ANOVA, $P < 0.0001$. *, $P < 0.01$, Tukey HSD test compared with CTRL, EV, or EV-IL30shRNA (clones D and B). **E,** IL30 immunostaining in normal prostate, PIN (11 weeks), and in poorly differentiated tumor (28 weeks) of TRAMP mice. IL30 (brown) colocalizes with Sca-1 (red) in PIN; scale bars, 50 μm (left two); 30 μm (right two and inset). **F,** Expression of IL6Rα and gp130 in PIN and in poorly differentiated adenocarcinoma (AC) of TRAMP mice; scale bars, 50 μm (left two); 30 μm (right two). **G,** IL30 immunostaining in normal prostate, PIN (IL30/CD133 colocalization), and in poorly differentiated adenocarcinoma; scale bars, 20 μm (left two and inset); 30 μm (right two).

paracrine or autocrine cytokine loops. The subcutaneous implantation of tumor cells allow for a precise measurement of the mean tumor volume (MTV) and mean latency time (MLT).

In the first set of experiments, three groups of mice were subcutaneously inoculated with 2×10^4 of PIN-SCs, or EV-IL30PIN-SCs, or IL30PIN-SCs (Fig. 2I and J). The first tumor mass

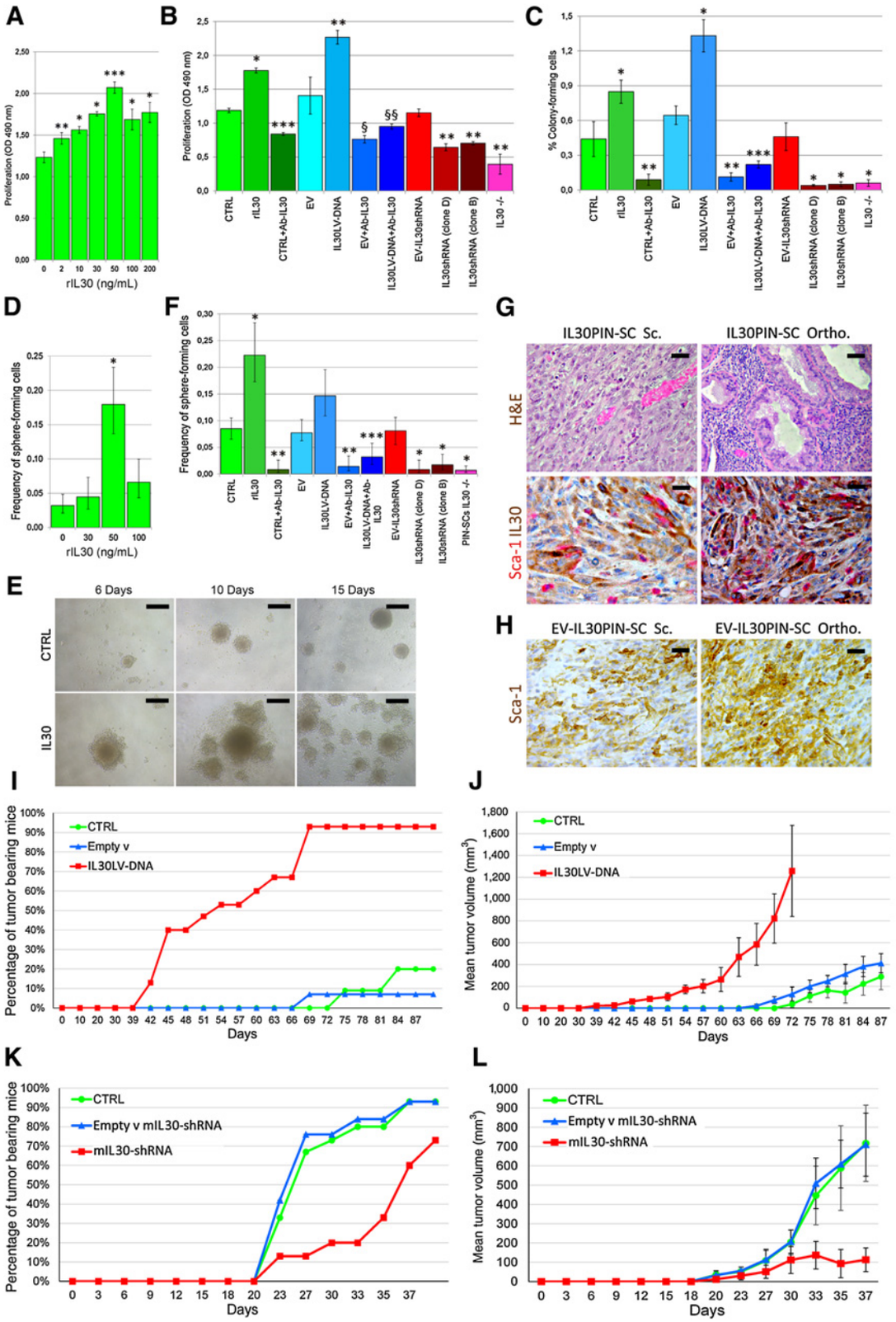

Table 1. Tumorigenicity of PIN-SCs implanted in congenic host

	Subcutaneous		*Orthotopic*			
	PIN-SCs		PIN-SCs		IL30PIN-SCs	
Cell number	Efficiency (%)	Tumor onset time (days)	Efficiency (%)	Tumor onset time (days)	Efficiency (%)	Tumor onset time (days)
2×10^6	100	18	—	—	—	—
5×10^4	100	28	—	—	—	—
4×10^4	70	55	—	—	—	—
3×10^4	60	63	—	—	—	—
2×10^4	20	68	50	60	85	48
1×10^4	—	—	40	70	78	61
5×10^3	—	—	20	84	45	76
1×10^3	—	—	10	95	20	86
1×10^1	—	—	5	120	10	105

to appear, after 39 days, was in the group of mice injected with IL30PIN-SCs. Ninety-three percent (42/45) of these mice developed a tumor with a 52 days MLT. Thus, the tumor take was significantly higher (ANOVA, $P < 0.0001$; Tukey HSD test, $P < 0.01$ vs. both controls) and the MLT considerably shorter (ANOVA, $P < 0.0001$; Tukey HSD test $P < 0.05$ vs. both controls) than what was observed in mice inoculated with PIN-SCs or EV-IL30PIN-SCs, which developed tumors in 9/45 and 3/45 cases, respectively, after 77 and 66 days MLT. Furthermore, the mean volume of the tumors developed after IL30PIN-SC injection was significantly higher (ANOVA, $P < 0.0001$; Tukey HSD test, $P < 0.01$ vs. both controls) than that observed in control mice.

In the second set of experiments, the consequences of blocking endogenous IL30 on the tumorigenic capability of PIN-SCs was assessed by subcutaneous inoculations of IL30shPIN-SCs, or EV-IL30shPIN-SCs, or PIN-SCs (1×10^5 cells, which allows 100% tumor take). As shown (Fig. 2K and L), 27% of mice inoculated with IL30shPIN-SCs did not develop any tumor, whereas the remaining (33/45; 73%) developed very small tumors with a MTV significantly lower than in controls (ANOVA, $P < 0.0001$; Tukey HSD test, $P < 0.01$ vs. both controls) and with a significantly longer MLT (32 days), than in mice injected with PIN-SCs (23 days), or EV-IL30shPIN-SCs (23 days; ANOVA, $P < 0.0001$; Tukey HSD test, $P < 0.01$ vs. both controls). The tumor take of IL30sh-PIN-SCs was considerably reduced in comparison with EV-IL30shPIN-SCs (42/45; 93%), or PIN-SCs (44/45; 98%; ANOVA, $P < 0.001$; Tukey HSD test, $P < 0.01$ vs. both controls).

Therefore, in a congenic immunocompetent host, IL30 substantially increased PCSLC capability to generate a tumor and sustain its development, whereas blocking its production consistently weakened PIN-SC tumorigenicity.

PCNA immunostaining revealed that IL30PIN-SC tumors had a higher proliferation index than controls (87.0% ± 8.2% vs. EV-IL30PIN-SC, 69.0% ± 6.5% and PIN-SC tumors, 66.7% ± 8.0%; ANOVA, $P < 0.05$; Tukey HSD test, $P < 0.05$ vs. both controls). By contrast, the proliferation index was consistently decreased in IL30shPIN-SC tumors (39.5% ± 7.0%) versus EV-IL30shPIN-SC (70.0% ± 6.2%) and PIN-SC tumors (ANOVA, $P < 0.05$; Tukey HSD test, $P < 0.05$ vs. both controls). Apoptotic events, assessed by TUNEL, were substantially unchanged in both IL30-PIN-SC (5.5% ± 2.7% vs. EV-IL30PIN-SC, 7.6% ± 3.8%) or IL30sh-PIN-SC tumors (12.5% ± 4.4% vs. EV-IL30shPIN-SC, 6.0% ± 3.5%; ANOVA, $P < 0.05$; Tukey HSD test, $P < 0.05$; Fig. 3A). Vascularization was prominent in IL30PIN-SC tumors (mean number of microvessels; MVD, 29.7 ± 6.3 vs. EV-IL30PIN-SC, 17.5 ± 4.0 and PIN-SC tumors, 18.0 ± 4.7; ANOVA, $P < 0.05$; Tukey HSD test, $P < 0.05$ vs. both controls). Furthermore, as observed in IL30–conditioned breast cancer (16), the vascular network showed an aberrant architecture characterized by ectatic endothelial branches, frequently encircling wide cancer cell emboli. By contrast, the vascular network appeared fairly pruned in IL30-silenced tumors (MVD, 7.8 ± 3.4 vs. 17.9 ± 5.2 in EV-IL30shPIN-SC tumors; ANOVA, $P < 0.05$; Tukey HSD test, $P < 0.05$ vs. both controls).

Along with a stronger IL30 production (Fig. 3B), IL30–overexpressing tumors were enriched in Sca-1^+ cells, when compared with controls. Their immune cell infiltrate was prominent and mainly constituted of F4/80^+macrophages, CD11b^+myeloid

Figure 2.

Effects of IL30 on PCSLC proliferation, self-renewal, and tumorigenicity. **A,** MTT assay of PIN-SCs 48 hours after rIL30 treatment. ANOVA, $P < 0.0001$. *, $P < 0.01$, Tukey HSD test compared with untreated PIN-SCs. **, $P < 0.05$, Tukey HSD test compared with untreated PIN-SCs. ***, $P < 0.01$, Tukey HSD test compared with PIN-SCs untreated and treated with rIL30 at 2, 10, 30,100, and 200 ng/mL. **B,** MTT assay of PIN-SCs after treatment with rIL30 (50 ng/mL), or IL30 overexpression, silencing, or knockout. ANOVA, $P < 0.0001$. *, Tukey HSD test compared with CTRL and EV-IL30shRNA ($P < 0.01$) or EV ($P < 0.05$). **, $P < 0.01$, Tukey HSD test compared with CTRL, EV, or EV-IL30shRNA. ***, Tukey HSD test compared with CTRL ($P < 0.05$) or EV ($P < 0.01$). §, $P < 0.01$, Tukey HSD test compared with CTRL or EV. §§, $P < 0.01$, Tukey HSD test compared with EV or IL30LV-DNA. **C,** Colony formation of PIN-SCs after treatment with rIL30 (50 ng/mL), or IL30 overexpression, silencing, or knockout. ANOVA, $P < 0.0001$. *, $P < 0.01$, Tukey HSD test compared with CTRL, EV, EV-IL30shRNA. **, $P < 0.01$, Tukey HSD test compared with CTRL or EV. ***, $P < 0.01$, Tukey HSD test compared with EV or IL30LV-DNA. **D,** Sphere-forming capability of PIN-SCs (by ELDA, $P < 0.0001$) 15 days after treatment with rIL30. *, $P < 0.01$, χ^2 test compared with untreated PIN-SCs, or treated with 30 or 100 ng/mL. **E,** PIN-SC–derived spheres were dissociated, seeded at concentrations of 1 cell/well, and treated with or without rIL30 (50 ng/mL); scale bars, 100 μm. **F,** Sphere-forming capabilities (by ELDA, $P < 0.0001$) of PIN-SCs after treatment with rIL30 (50 ng/mL), or IL30 overexpression, silencing (clones D and B), or knockout. *, $P < 0.01$, χ^2 test compared with CTRL, EV, or EV-IL30shRNA. **, $P < 0.01$, χ^2 test compared with CTRL or EV. ***, $P < 0.01$, χ^2 test compared with EV or IL30LV-DNA. **G,** Histology and immunohistochemistry (IL30/Sca-1 colocalization) of subcutaneous and orthotopic IL30PIN-SC tumors; scale bars, 50 μm (top right); 30 μm (top left); 20 μm (bottom). **H,** Sca-1 immunostaining of subcutaneous and orthotopic EV-IL30PIN-SC tumors; scale bars, 30 μm. **I** and **K,** Percentage of tumors developed after implantation of IL30–overexpressing (**I**) or IL30-silenced (**K**) PIN-SCs (ANOVA, $P < 0.001$; Tukey HSD test, $P < 0.01$ vs. both controls). **J** and **L,** Mean volume of tumors developed after implantation of IL30–overexpressing (**J**) or IL30–silenced (**L**) PIN-SCs (ANOVA, $P < 0.0001$; Tukey HSD test, $P < 0.01$ vs. both controls). H&E, hematoxylin and eosin.

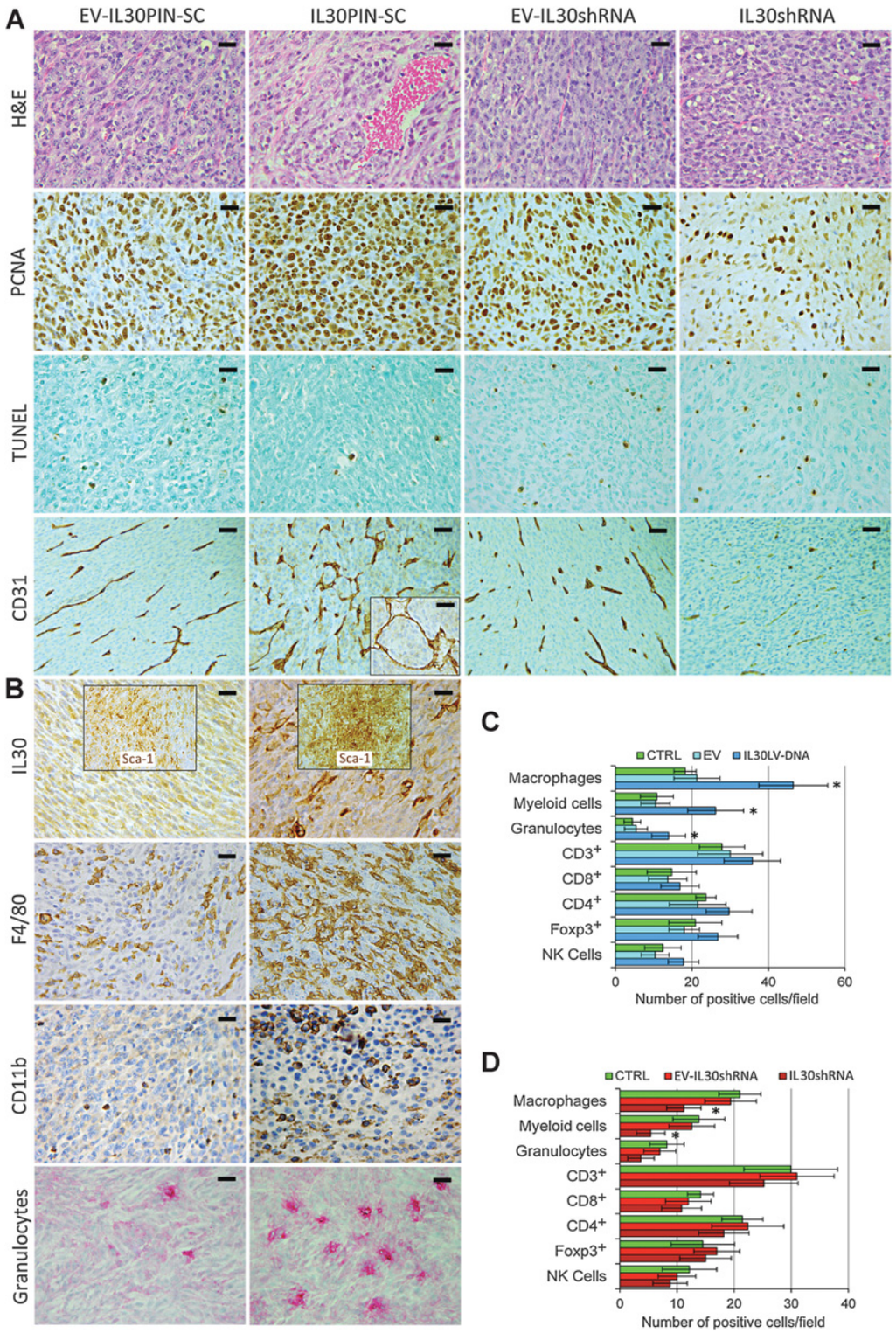

Figure 3.

Effects of IL30 overproduction or silencing on subcutaneous PCSLC-derived tumors. **A,** Histology and immunohistochemistry of IL30PIN-SC and IL30shPIN-SC tumors versus controls; scale bars, 50 μm (bottom); 30 μm (other and inset). **B,** Immunohistochemical features of IL30PIN-SC and EV-IL30PIN-SC tumors; scale bars, 30 μm; 20 μm (granulocytes). **C** and **D,** Immune cells in IL30–overexpressing (**C**) or IL30-silenced (**D**) PIN-SC tumors. Results are expressed as mean ± SD of positive cells/field evaluated at ×400 (0.180 mm^2 field) by immunohistochemistry. *, values significantly ($P < 0.05$) different from controls. H&E, hematoxylin and eosin.

cells, and Ly-6G$^+$granulocytes. These leukocyte populations were poorly represented inside IL30–silenced tumors when compared with controls, whereas the number of CD3$^+$T lymphocytes (both CD8$^+$ and CD4$^+$), Foxp3$^+$Tregs and NKp46 cells was substantially unchanged in both IL30–overexpressing and IL30-silenced tumors when compared with controls (Fig. 3B–D).

IL30 regulates PCSLC expression of genes involved in inflammation, immune-suppression and metastasis, mostly via STAT1/STAT3 signaling

The intratumoral reactive cell recruitment found in IL30–conditioned tumors lead to the assessment of IL30's capability to regulate, in PCSLCs, the expression of genes implicated in inflammation and immune cell crosstalk.

Stimulation of PIN-SCs with rIL30 upregulated chemokines, such as *Ccl4* (5.92-times), *Ccl20* (3.9-times), *Cxcl1* (3.02-times), *Cxcl2* (3.05-times), *Cxcl9* (3.19-times), and *Cxcl10* (3.30-times), whereas *Cxcl5*, *Cxcl11* and *Cxcl12* were downmodulated (7.11, 3.62, and 9.99-times, respectively). IL30 also promoted the expression of inflammatory mediators and growth factors, such as *IL6* (3.5-times), *IL15* (2.71-times), *Csf3* (2.8-times), *Spp1/osteopontin* (2.14-times), *Ptgs2* (4.0-times), *Vegfa* (2.37-times), *Egf* (4.21-times) and, especially, *IL1α* (7.67-times), *IL1β* (5.35-times), *Csf2* (5.08-times) and *Tnfα* (15.45-times), whereas *IL5*, *IL23α* and *Egfr* were downregulated (2.69, 2.84, and 3.06-times; Fig. 4A).

Interestingly, expression of interferon–inducible guanylate-binding protein *2b* (Gbp2b) was consistently reduced (15.0-times), whereas expression of *Cd274/PD-L1* and *Foxp3* was increased (3.18 and 3.32-times, respectively), along with *H2-d1* (2.72 times), *Myd88* (2.60-times), and most of all Toll-like-receptor-*3 (Tlr3*; 9.68-times) and the *c-Kit ligand (Kitl*; 17.69-times; Fig. 4A). Furthermore, IL30 treatment greatly increased PIN-SC's expression of chemokine receptors *Ccr1* (52.0-times), *Cxcr1* (13.0-times), *Cxcr4* (17.39-times), and *Cxcr5* (34.9-times; Fig. 4A).

Furthermore, silencing of endogenous IL30, in PIN-SCs, suppressed the expression of the genes primarily regulated by IL30, such as *Ccr1*, *Cxcl2*, *Cxcr1*, *Cxcr4*, *Cxcr5*, *Kitl* and *Tnfα*, whereas it upregulated *Cxcl12* (Fig. 4B).

Immunohistochemistry substantiated PCR array data, revealing a distinct to strong expression of IL1β, Tnfα, IL6, Csf2, Cxcl2, Egf and Cd274/PD-L1 in IL30PIN-SC tumors, when compared with controls (Fig. 4C). Increased *PD-L1* expression not only involved cancer cells in IL30PIN-SC tumor, but also tumor- and draining LN-infiltrating immune cells (Fig. 4D). IL30—overexpressing tumors also revealed a remarkable cancer cell expression of Ccr1, Cxcr4, and Cxcr5, which was scanty in control tumors (Fig. 4E).

Because the engagement of gp130 by IL30 (20, 22), activates the Janus family kinases and leads to the recruitment, phosphorylation and activation of STAT1 and STAT3, and because we detected an increase in their phosphorylation (p) status in PIN-SCs following IL30 stimulation (Supplementary Fig. S6), we proceeded to knockdown these transcription factors (Fig. 4F) and to assess their involvement in IL30–dependent regulation of the major inflammatory mediators and tumor progression genes. Silencing of both *Stat1* and *Stat3* substantially ($P < 0.05$) hampered or abolished the genes primarily regulated by IL30, except for *IL1β, Csf2 and Cxcl1* whose expression was affected by Stat3 silencing only (Fig. 4G). In particular, IL30-dependent upregulation of *Ccl4*, *Csf2*, *Cxcl1*, *Cxcl2*, *Cxcr4*, *IL1α*, *Tnfα and Vegfa* was abolished by *Stat3* knockdown, whereas the upregulation of *Egf* was abolished by *Stat1* knockdown-(Fig. 4G and H; ref. 23).

IL30 conditioning of orthotopically implanted PCSLCs promotes their metastasis to the lung, which involves the CXCL12/CXCR4 axis

IL30's ability to boost, *in vitro* and *in vivo*, in PIN-SC the expression of genes involved in inflammation, tumor progression and metastasis, prompted us to investigate whether IL30 conditioning of the prostate microenvironment could affect PCSLCs spread to distant organs. To this aim, three groups of mice underwent intra-prostatic implantation of IL30PIN-SCs (1×10^4, able to generate tumor in 78% of mice) or EV-IL30PIN-SCs or PIN-SCs (4×10^4 cells, able to generate tumor in 80% of mice). Thus, for each group, a number of cells resulting in a comparable tumor take was used and mice were maintained until evidence of suffering was observed (about 80 days).

Autopsy of mice and histopathological analyses (prostate, pelvic LNs, spleen, liver, lungs, spinal column, and bone marrow) revealed that the lungs were the favorite site of PIN-SC metastasis. The number of mice with lung metastases was significantly greater in the group of mice bearing intraprostatic IL30–overexpressing tumors (tumor take 33/45; 73%). In fact, 82% (27/33) of these mice developed metastasis, whereas only 46% (16/35) of mice bearing EV-IL30PIN-SC tumors (tumor take 35/45; 78%) and 52% (16/31) of mice bearing PIN-SC tumors (tumor take 31/45; 69%) developed metastasis (ANOVA, $P = 0.025572$; Tukey HSD test, $P < 0.05$ vs. both controls). In all mice, metastasis arose as sub-pleural and peri-bronchial neoplastic infiltrates, which were wider in mice bearing IL30-overexpressing tumors (Fig. 5A). Intriguingly, immunohistochemistry revealed a strong expression of the CXCR4 ligand, CXCL12 (24), typically in the mesothelium and in the pseudo-stratified epithelium lining the inner bronchial walls, in lungs with or without metastasis, developed from IL30- or EV-IL30PIN-SC tumor-bearing mice (such as in lungs from control tumor free mice). However, IL30–conditioned lung metastases, such as the tumor of origin, strongly expressed CXCR4, whereas metastasis from EV-IL30PIN-SC tumors showed a scanty CXCR4 expression (Fig. 5B). CXCL12 expression was barely detected in the prostate draining LNs and in bone marrow from all mouse groups.

To assess the involvement of CXCR4/CXCL12 in the higher propensity to lung metastasis of IL30PIN-SCs versus EV-IL30PIN-SCs, we analyzed the chemotactic response of PIN-SCs toward CXCL12, following their treatment with rIL30 or IL30PIN-SCsup (Fig. 5C). The number of PIN-SCs that migrated toward CXCL12 was significantly higher after 48 hours pretreatment with rIL30 (50 ng/mL) or IL30PIN-SCsup. Addition of anti–IL30Abs to IL30PIN-SCsup–treated PIN-SCs significantly decreased ($P < 0.05$), but did not abolish, their migration toward CXCL12. Indeed, the chemotactic response of IL30–treated PIN-SCs to CXCL12, increased with IL30 concentration (from 50 to 200 ng/mL). The CXCL12 dependent chemotaxis of PIN-SCs, induced by rIL30 or IL30PIN-SCsup, was abrogated by anti-CXCR4 Abs, whereas it was maintained in the presence of isotype control Abs, thus supporting a role for CXCR4 upregulation in IL30–dependent PIN-SC colonization of the lungs.

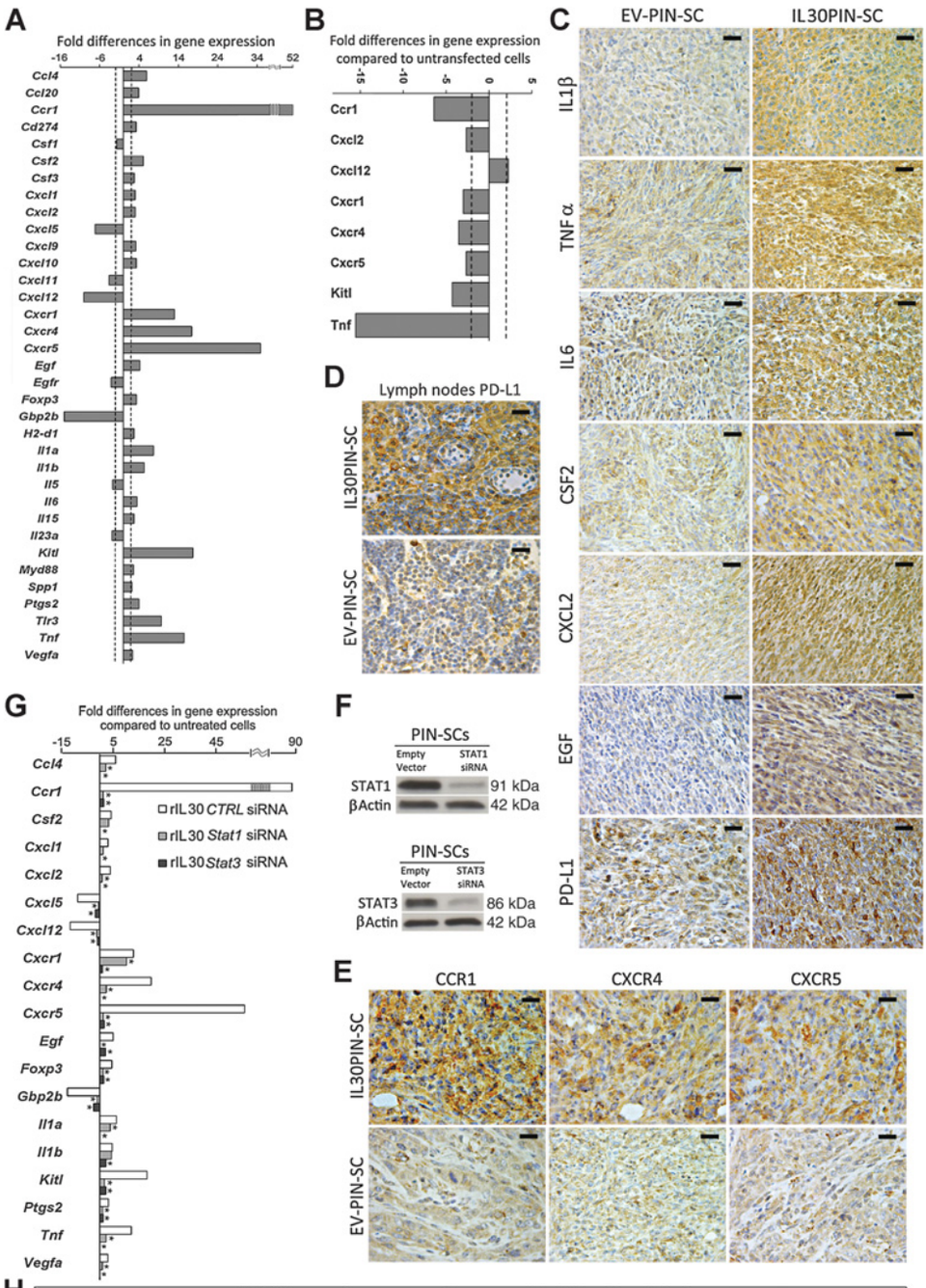

Fold differences in gene expression compared to rIL30 only treated cells

	Ccl4	Ccr1	Csf2	Cxcl1	Cxcl2	Cxcl5	Cxcl12	Cxcr1	Cxcr4	Cxcr5	Egf	Foxp3	Gbp2b	Il1a	Il1b	Kitl	Ptgs2	Tnf	Vegfa
Stat1 siRNA	-3,85	-87,17	-0,95	-1,88	-3,12	8,09	10,31	-2,66	-17,42	-54,67	0	-3,47	11,56	-2,43	-0,3	-16,43	-2,26	-9,77	-2,07
Stat3 siRNA	0	-86,84	0	0	0	6,88	10,46	-11,96	-19,879	-54,33	-2,96	-3,11	10,2	0	-2,4	-15,82	-2,08	0	0

Figure 4.

IL30's ability to regulate gene expression of PCSLCs and PCSLC-derived tumors. **A,** Fold differences of mRNAs between rIL30–treated and untreated PIN-SCs. A significant threshold of 2-fold change in gene expression corresponded to $P < 0.001$. **B,** Fold differences of mRNAs between IL30shPIN-SCs and EV-IL30shPIN-SCs. Results from the latter are comparable to those from untransfected cells. A significant threshold of 2-fold change in gene expression corresponded to $P < 0.001$. **C–E,** Immunohistochemical features of prostate draining LNs, IL30PIN-SC, and EV-IL30PIN-SC orthotopic tumors; scale bars, 30 μm. **F,** Silencing of STAT1 and STAT3 in PIN-SCs, as confirmed by Western blot. **G,** Fold differences of mRNAs between *Stat1* siRNA- or *Stat3* siRNA- or CTRL siRNA-transfected PIN-SCs cultured with rIL30 and untreated CTRL siRNA-transfected PIN-SCs. Results from the latter are comparable with those from untreated and untransfected cells. A significant threshold of 2-fold change in gene expression corresponded to $P < 0.001$. *, $P < 0.05$ by Student *t* test compared with rIL30–treated CTRL siRNA-transfected PIN-SCs. **H,** Fold differences of mRNAs between *Stat1* siRNA- or *Stat3* siRNA-transfected PIN-SCs cultured with rIL30 and rIL30–treated CTRL siRNA-transfected PIN-SCs. A significant threshold of 2-fold change in gene expression corresponded to $P < 0.001$.

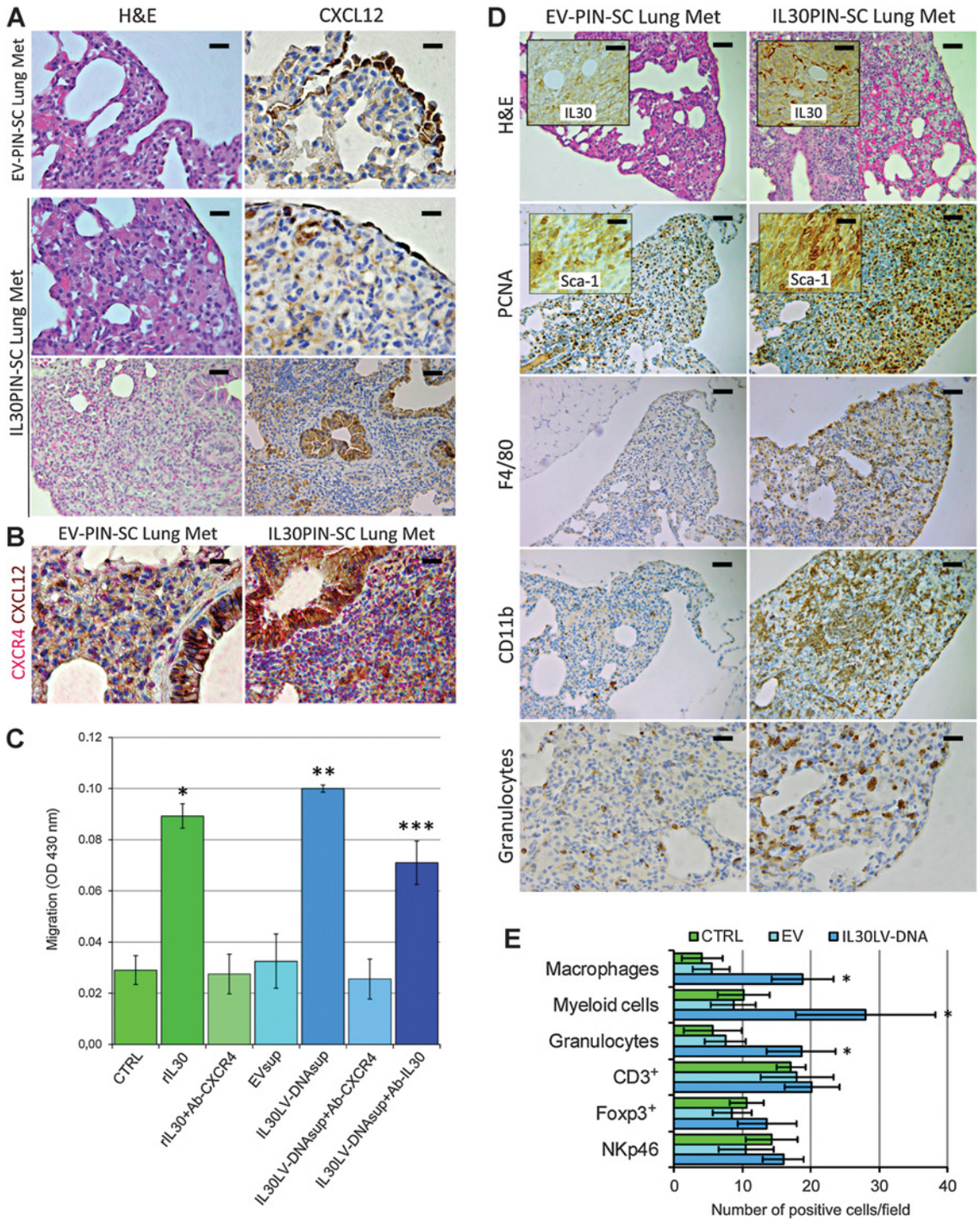

Figure 5.

IL30 favors PCSLC metastasis to the lungs involving CXCR4/CXCL12 axis. **A,** Histology and immunohistochemistry of lung metastasis in IL30PIN-SC and EV-IL30PIN-SC tumor bearing mice. Scale bars, 50 μm (bottom); 30 μm (other). **B,** Expression of CXCR4 and CXCL12 in lung metastasis developed in IL30PIN-SC and EV-IL30PIN-SC tumor-bearing mice; scale bars, 30 μm. **C,** Migration of IL30–treated PIN-SCs toward CXCL12. Results are expressed as mean ± SD. ANOVA, $P < 0.0001$. *, Tukey HSD test compared with CTRL and rIL30+Ab-CXCR4 ($P < 0.05$) or EVsup and IL30LV-DNAsup+Ab-CXCR4 ($P < 0.01$). **, $P < 0.01$, Tukey HSD test compared with CTRL, rIL30+Ab-CXCR4, EVsup, and IL30LV-DNAsup+Ab-CXCR4. ***, Tukey HSD test compared with CTRL, rIL30+Ab-CXCR4, EVsup, and IL30LV-DNAsup+Ab-CXCR4 ($P < 0.01$) or IL30LV-DNAsup ($P < 0.05$). **D,** Histology and immunohistochemistry of lung metastasis in mice bearing orthotopic IL30PIN-SC and EV-PIN-SC tumors; scale bars, 50 μm; 30 μm (bottom and insets). **E,** Immune cells in lung metastasis of mice bearing orthotopic IL30PIN-SC tumors versus controls. Results are expressed as mean ± SD of positive cells/field (×400) evaluated by immunohistochemistry. *, values significantly ($P < 0.05$) different from values in EV-PIN-SC and PIN-SC tumors. H&E, hematoxylin and eosin.

IL30–conditioned lung metastases were enriched in ectatic microvessels, when compared with metastases from EV-IL30PIN-SC tumors (Fig. 5D, hematoxylin and eosin). They were formed by highly proliferating ($PCNA^+$), and mostly Sca-1^+ cancer cells and revealed a consistent $CD11b^+$, Ly-$6G^+$ and $F4/80^+$ cell infiltrate when compared with controls (Fig. 5D and E).

The IL30 conditioning of orthotopically implanted PCSLCs favors their spread to the lymph nodes and bone marrow involving CXCR5/CXCL13 axis

Although the lungs appeared as the main site for metastatic outgrowth, dissemination of PCSLCs was found in both bone marrow and, particularly, pelvic LNs, more frequently in mice bearing intra-prostatic IL30PIN-SC tumors. These tumors diffusely grew within the prostatic ducts and encompassed the surrounding vessels, in which isolated Sca-1^+/$IL30^+$ cells were frequently visualized (Fig. 6A). This feature, in line with the high metastatic capability of IL30PIN-SC cells, raises the question of the mechanisms underlying IL30 promotion of PCSLC dissemination.

Interestingly, pelvic LNs draining IL30-conditioned tumors were usually larger, thus more easily detectable than LNs from control tumor-bearing mice. Their expansion was mainly due to hyperplasia of the sinuses histiocytes, mostly expressing CXCL13, and follicular B cell zone, which revealed wide germinal center containing tangles of $CXCL13^+$ follicular dendritic-like cells (Fig. 6B). Automated evaluation, by light microscopy, with Qwin Image analysis software, of CXCL13 expression (evaluated as the mean percentage $\pm$ SD of positively stained area/total area of the examined fields) in LNs draining prostatic tumors, revealed that it was substantially increased in LNs from mice bearing IL30PIN-SC tumors, when compared with LNs from mice bearing EV- IL30PIN-SC or PIN-SC tumors (20 ± 5 vs. 6 ± 4 and vs. 7 ± 3, respectively; ANOVA, $P < 0.05$; Tukey HSD test, $P < 0.05$ vs. both controls). Close to the CXCL13 expression, by germinal centers and by histiocyte-like cells, the turnout of $CK5/6^+$ cancer cells (evaluated, by light microscopy with Qwin software, as the mean $\pm$ SD of positive cells/field; ref. 25) was prominent in LNs draining IL30PIN-SC tumors, than in LNs draining EV-IL30PIN-SC or PIN-SC tumors (43 ± 14 vs. 12 ± 7 and 11 ± 5, respectively; ANOVA, $P < 0.05$; Tukey HSD test, $P < 0.05$ vs. both controls). $CK5/6^+$ cells, detected in LNs draining IL30PIN-SC tumors or EV-IL30PIN-SC tumors, coexpressed Sca-1, which indicates that they were PCSLCs (Fig. 6B).

In addition, vertebral bone marrow from mice bearing IL30–overexpressing or control tumors, revealed scattered $CK5/6^+$ cells more frequently in mice bearing IL30PIN-SC tumors, and close to $CXCL13^+$ stromal cells endowed with macrophage- and osteoblastic-like feature (Fig. 6C).

The chemokine CXCL13 is the only ligand for CXCR5 (26), which was consistently up-regulated in IL30–treated PIN-SCs and in IL30PIN-SC tumors. Thus, we tested the chemotactic response of PIN-SCs to CXCL13, after treatment with rIL30 or with IL30PIN-SCsup (Fig. 6D). The number of PIN-SCs, which migrated toward CXCL13, was significantly higher, after 48 hours treatment with rIL30 (50 ng/mL) or IL30PIN-SCsup, which effect was vanished by the addition of anti–IL30Abs to the medium. The chemotactic response of IL30-treated PIN-SCs to CXCL13, increased with IL30 concentration (from 50 to 200 ng/mL). Chemotaxis toward CXCL13, promoted by rIL30 or IL30PIN-SCsup, was abrogated by anti-CXCR5Abs, thus highlighting the role of CXCR5 upregulation in IL30–dependent PIN-SC migration and dissemination.

Discussion

Originally identified in activated monocytes and dendritic cells, in humans, in the thymus and in activated macrophages, in mice (11), IL30, has been recognized with its own immunological identity demonstrating anti-inflammatory (27) and antifibrotic effects (28), and the ability to suppress autoimmunity (29). However, it may also reveal a pro-inflammatory potential, because it is known to signal, like IL6, via IL6Rα by recruiting a gp130 homodimer (20).

Recently, we found that IL30 is produced in breast and prostate cancers, by both cancer cells and tumor- or LN-infiltrating leukocytes, mostly myeloid cells, particularly in high-grade and stage of the diseases (13, 16). The present study has made a step forward in understanding IL30's role in prostate cancer biology by disclosing autocrine and paracrine pathways triggered by the cytokine to shape the fate of PCSLCs in an orthotopic immune-competent model, which closely mimics a real "PCSLC niche microenvironment."

In the TRAMP model, as observed in prostate cancer patients, IL30 is produced by the majority of cancer cells in high-grade, poorly differentiated prostate cancer (13), whereas it is confined to PCSLCs in precursor lesions, such as PIN. Isolated from this lesion, PCSLCs, namely PIN-SCs, produce and release IL30, which can act at very low dosage on the cells themselves, because they express both gp130 and, although at low levels, IL6Rα (20), but also on the microenvironment when PIN-SCs are implanted into a congenic host. Almost devoid of EBI3, this tissue microenvironment prevents IL30 to engage IL27R on locally available leukocytes, and thus to act like IL27 (20).

As expected, PIN-SC better survive and give rise to a tumor, in the orthotopic rather than in the subcutaneous site, in which the stemness phenotype is no longer maintained. In both microenvironments, however, IL30 increases PCSLC tumorigenicity providing *in vivo* confirmation of its ability to boost PCSLC viability and self-renewal capability. These properties appear to be considerably weakened by silencing, with specific shRNA, or knocking out, with CRISPR/Cas9-based approach, the constitutive expression of the cytokine, thus strengthening its role as a novel PCSLC growth factor. The potential off-target effect was ruled out by the use of four independent shRNA constructs, and two guide RNA sequences, designed to selectively target *mIL30* gene, which resulted in comparable *in vitro* effects (30).

Furthermore, the peculiar expression profile of inflammation- and immunity-related genes shaped by IL30 in PCSLCs, reveals its ability to promote a pro-oncogenic and metastatic phenotype and to govern the intratumor immune cell homing.

Among the dominant traits of the subverted PCSLC phenotype is the strengthening of tumor immune-evasion strategies, such as the dramatic downmodulation of the expression of *Gbp2b*, an IFNγ inducible protein, which is controlled by p53 and may function as a tumor suppressor by inhibiting NFκB and Rac. It has been correlated with a T-cell signature and a better prognosis in fast proliferating tumors (31). Noteworthy is the IL30–mediated upregulation of *Cd274/PD-L1*, which is consistent with an

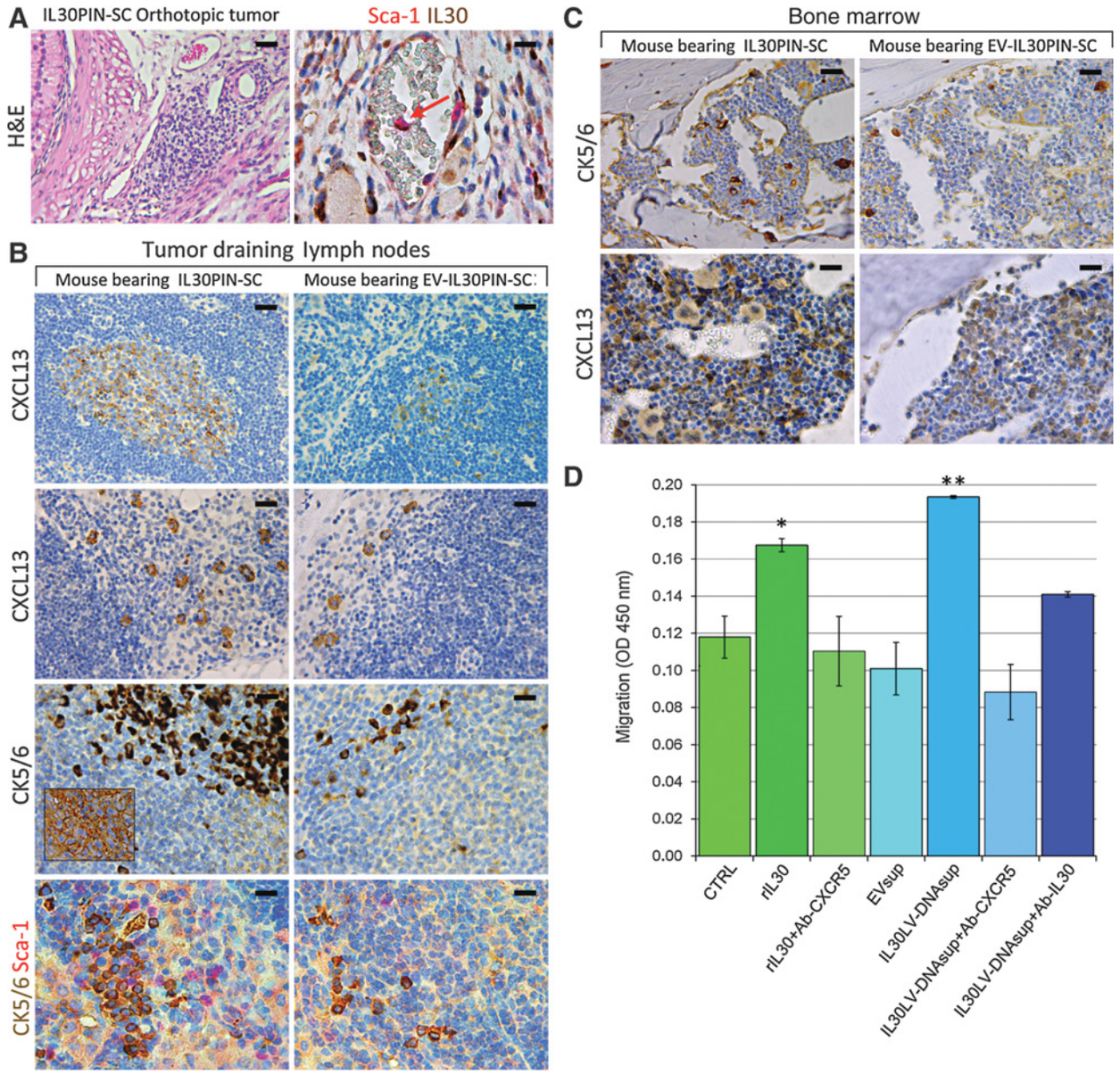

Figure 6.

IL30 promotes PCSLC dissemination in the LNs and bone marrow involving CXCR5/CXCL13 upregulation. **A,** Histology and immunohistochemistry of IL30PIN-SC orthotopic tumors. Isolated Sca-1$^+$/IL30$^+$ cells (red arrow) inside the blood vessels; scale bars, 50 μm (left); 20 μm (right). **B,** Immunohistochemistry of LNs draining IL30PIN-SC or EV-IL30PIN-SC orthotopic tumors. The inset shows CK5/6 staining of the primary tumor. In LNs, CK5/6$^+$ colocalizes with Sca-1; scale bars, 30 μm; 20 μm (bottom). **C,** Immunohistochemistry of bone marrow from mice bearing IL30PIN-SC and PIN-SC orthotopic tumors; scale bars, 50 μm (top); 30 μm (bottom). **D,** Migration of IL30–treated PIN-SCs toward CXCL13. Results are expressed as mean ± SD. ANOVA, $P < 0.0001$. *, Tukey HSD test compared with CTRL and rIL30+Ab-CXCR5 ($P < 0.05$) or EVsup and IL30LV-DNAsup+Ab-CXCR5 ($P < 0.01$). **, Tukey HSD test compared with CTRL, rIL30+Ab-CXCR5, EVsup, and IL30LV-DNAsup+Ab-CXCR5 ($P < 0.01$) or IL30LV-DNAsup ($P < 0.05$).

increased adaptive immune resistance (32, 33) and of *Foxp3*, which is believed to enable the immune evasion of cancer cells and has long been associated with worse prognosis in breast and pancreatic cancers (34, 35).

An impressive upregulation of *TLR3* and *Kitl*, was caused by IL30 in PCSLs. TLRs expressed by immune cells, play a crucial role in the innate and adaptive immune responses against microbial infection or tissue injury (36). However, activated TLR signals on cancer cells may promote cancer progression and resistance to host immune responses (37, 38). An ambiguous role has been ascribed to TLR3 when expressed by cancer cells, because its activation can trigger apoptosis as well as stimulate cancer cell survival, proliferation, and migration (39, 40) and also activate inflammatory-related molecules in

the TME (41). A robust expression of Kitl by cancer cells has been demonstrated to promote intratumoral Kit^+CD11b^+ cell recruitment, which also occurs inside IL30–conditioned PIN-SC tumors, whereas blocking of the Kitl/Kit axis slows-down tumor progression and metastasis (42), thus suggesting it as one of the mechanisms underlying IL30–driven tumor progression.

Together with a prominent expression of *Kitl*, *TLR3* and PD-L1, able to oppose any host's attempt of mounting an antitumor immune response, IL30 unbalances the TME toward a pro-inflammatory and angiogenic milieu dominated by *IL1α*, *IL1β*, *IL6*, *Csf2*, *Ptgs2* and most of all of *Tnfα*, which may directly affect tumor cell survival, but also have a role in immune cell recruitment and pro-tumoral functions (43).

The intra-tumoral immune cell profile dictated by IL30, which is mostly composed of macrophages, granulocytes and myeloid derived cells, fits well with its ability to boost cancer cell expression of a variety of chemokines, mostly myeloid cell chemoattractants, such as *Ccl4*, *Ccl20*, *Cxcl1*, *Cxcl2*, *Csf2*, *Csf3* (24, 44), whereas the expression of *Cxcl5*, *Cxcl11* and, particularly of the lymphocyte chemoattractant *Cxcl12* (24) was inhibited.

STAT1 and STAT3 signaling are both involved in IL30's shaping of the TME, because the pro-oncogenic and -inflammatory program fostered by IL30 in PCSLCs is hindered or abolished by knock-down of these transcription factors, with a relevant role for the STAT3 pathway (23) in the regulation of a range of genes crucial for cancer inflammation, vascularization and immune cell recruitment such as, *IL1α* and *β*, *Tnfα*, *Vegfa*, *Ccl4*, *Csf2*, *Cxcl1*, *Cxcl2*, and *Cxcr4*.

A prevalent myeloid cell infiltrate and a robust network of ectatic microvessels, along with several secondary mediators, previously demonstrated in IL30–treated mammary tumor xenografts (16), are also the hallmark of IL30–driven tumor growth and metastasis in the present PCSLC model. Indeed, they characterize both the primary tumor and lung metastasis and become heavily compromised, together with tumor progression, when PCSLC production of IL30 is silenced. Expression of growth factors, angiogenic and angiostatic mediators, such as *Egf, Vegfa* (45), *Spp1* (46), *Cxcl9, and Cxcl10* (24) is promoted by IL30 in PCSLs and may cooperate in conditioning their niche microenvironment and their behavior. Certainly, IL30 confers PCSLC with striking migration ability by greatly improving their expression of chemokine receptors, in particular, *Ccr1*, *Cxcr1*, *Cxcr4*, and *Cxcr5* (47).

Although the role of CCR1 and CXCR1, which may interact with multiple ligands, remains to be investigated, here we demonstrated that IL30 promotes PCSLC migration toward CXCL13 and CXCL12, which is prevented by blocking, respectively, CXCR5 and CXCR4.

In vivo, IL30 overexpression by the primary tumor favors PCSLC spread to the draining lymph nodes and bone marrow, by boosting both the local production of CXCL13, which creates a pre-metastatic niche microenvironment (48), and PCSLC expression of CXCR5 (49, 50). IL30 overexpression by the primary tumor also strengthens PCSLC propensity for lung colonization, which involves CXCR4 and takes place, selectively, close to the $CXCL12^+$ pleural covering and bronchiolar walls. Interestingly, *in vitro* experiments suggest that migration of PCSLCs toward CXCL12 does not just rely on IL30 *per se*, but might be due to secondary mediators autocrinally induced, because it is not abolished by adding IL30Abs.

Although many aspects of the role of IL30 in prostate cancer onset and progression and, specifically, in regulating PCSLCs, such as its effects on the different components of the articulated TME, remains to be elucidated, the present study demonstrates, for the first time, that IL30 functions as an autocrine growth factor for PCSLCs by directly supporting their viability, self-renewal and migratory abilities, and strengthening their tumorigenicity in a fully immunocompetent host, while preparing an "ad hoc" premetastatic niche in the lymph nodes and bone marrow that helps their systemic dissemination. The role of STAT3 in prostate carcinogenesis is currently highly debated, because contrasting data emerged from different studies (51–53). In the clinical practice, the genetic and microenvironmental tumor heterogeneity may condition patient outcomes (54), by regulating cancer cell plasticity and CSLC content. It is established that the IL6/STAT3 pathway is crucial for the maintenance of the Stem Cell phenotype in prostate cancer (55, 56) and this justifies the importance of pursuing the successful targeting of STAT3 in PCSLCs *in vivo* (57). It is widely recognized that prostate cancer recurrence and lethality is due to a small population of PCSLCs and their exit from a steady state condition is driven by microenvironmental and autocrine signals. Among these, IL30/IL6R/gp130 axis has now revealed to be a key player in shaping PCSLC behavior and metastatic potential. This new finding could help explain the failure of an anti–IL6 Ab monotherapy with siltuximab in metastatic castration-resistant prostate cancer patients (58), and further warrants a study to target IL6R, also blocking IL30 signaling.

Suppressing PCSLC aggressiveness by selectively targeting an upstream driver of their tumorigenicity could be translated into an effective strategy to hinder prostate cancer progression or recurrence with relevant clinical implications.

Disclosure of Potential Conflicts of Interest

No potential conflicts of interest were disclosed.

Authors' Contributions

Conception and design: E. Di Carlo
Development of methodology: C. Sorrentino, S.L. Ciummo
Acquisition of data (provided animals, acquired and managed patients, provided facilities, etc.): M. Bellone
Analysis and interpretation of data (e.g., statistical analysis, biostatistics, computational analysis): C. Sorrentino, S.L. Ciummo, E. Di Carlo
Writing, review, and/or revision of the manuscript: C. Sorrentino, E. Di Carlo
Administrative, technical, or material support (i.e., reporting or organizing data, constructing databases): G. Cipollone, S. Caputo
Study supervision: E. Di Carlo

Acknowledgments

This work was supported by grants from the Italian Ministry of Health, Ricerca Finalizzata (RF-2013-02357552 to E. Di Carlo) and Associazione Italiana Ricerca sul Cancro (IG-16807 to M. Bellone).

The costs of publication of this article were defrayed in part by the payment of page charges. This article must therefore be hereby marked *advertisement* in accordance with 18 U.S.C. Section 1734 solely to indicate this fact.

Received October 10, 2017; revised December 1, 2017; accepted February 22, 2018; published first February 27, 2018.

References

1. Torre LA, Bray F, Siegel RL, Ferlay J, Lortet-Tieulent J, Jemal A. Global cancer statistics, 2012. CA Cancer J Clin 2015;65:87–108.
2. Sampieri K, Fodde R. Cancer stem cells and metastasis. Semin Cancer Biol 2012;22:187–93.
3. Plaks V, Kong N, Werb Z. The cancer stem cell niche: how essential is the niche in regulating stemness of tumor cells? Cell Stem Cell 2015; 16:225–38.
4. Hanahan D, Coussens LM. Accessories to the crime: functions of cells recruited to the tumor microenvironment. Cancer Cell 2012;21:309–22.
5. Mateo F, Meca-Cortés O, Celià-Terrassa T, Fernández Y, Abasolo I, Sánchez-Cid L, et al. SPARC mediates metastatic cooperation between CSC and non-CSC prostate cancer cell subpopulations. Mol Cancer 2014;13:237.
6. Shiozawa Y, Havens AM, Jung Y, Ziegler AM, Pedersen EA, Wang J, et al. Annexin II/annexin II receptor axis regulates adhesion, migration, homing, and growth of prostate cancer. J Cell Biochem 2008;105:370–80.
7. Mathieu J, Zhang Z, Zhou W, Wang AJ, Heddleston JM, Pinna CM, et al. HIF induces human embryonic stem cell markers in cancer cells. Cancer Res 2011;71:4640–52.
8. Goel HL, Chang C, Pursell B, Leav I, Lyle S, Xi HS, et al. VEGF/neuropilin-2 regulation of Bmi-1 and consequent repression of IGF-IR define a novel mechanism of aggressive prostate cancer. Cancer Discov 2012;2:906–21.
9. Kobayashi A, Okuda H, Xing F, Pandey PR, Watabe M, Hirota S, et al. Bone morphogenetic protein 7 in dormancy and metastasis of prostate cancer stem-like cells in bone. J Exp Med 2011;208:2641–55.
10. Sun X, Cheng G, Hao M, Zheng J, Zhou X, Zhang J, et al. CXCL12/CXCR4/CXCR7 chemokine axis and cancer progression. Cancer Metastasis Rev 2010;29:709–22.
11. Pflanz S, Timans JC, Cheung J, Rosales R, Kanzler H, Gilbert J, et al. IL-27, a heterodimeric cytokine composed of EBI3 and p28 protein, induces proliferation of naive CD4+ T cells. Immunity 2002;16:779–90.
12. Di Carlo E. Interleukin-30: a novel microenvironmental hallmark of prostate cancer progression. Oncoimmunology 2014;3:e27618.
13. Di Meo S, Airoldi I, Sorrentino C, Zorzoli A, Esposito S, Di Carlo E. Interleukin-30 expression in prostate cancer and its draining lymph nodes correlates with advanced grade and stage. Clin Cancer Res 2014;20:585–94.
14. Mazzoleni S, Jachetti E, Morosini S, Grioni M, Piras IS, Pala M, et al. Gene signatures distinguish stage-specific prostate cancer stem cells isolated from transgenic adenocarcinoma of the mouse prostate lesions and predict the malignancy of human tumors. Stem Cells Transl Med 2013;2:678–89.
15. Hu Y, Smyth GK. ELDA: extreme limiting dilution analysis for comparing depleted and enriched populations in stem cell and other assays. J Immunol Methods 2009;347:70–8.
16. Airoldi I, Cocco C, Sorrentino C, Angelucci D, Di Meo S, Manzoli L, et al. Interleukin-30 promotes breast cancer growth and progression. Cancer Res 2016;76:6218–29.
17. Kaplan-Lefko PJ, Chen TM, Ittmann MM, Barrios RJ, Ayala GE, Huss WJ, et al. Pathobiology of autochthonous prostate cancer in a pre-clinical transgenic mouse model. Prostate 2003;55:219–37.
18. Greenberg NM, DeMayo F, Finegold MJ, Medina D, Tilley WD, Aspinall JO, et al. Prostate cancer in a transgenic mouse. Proc Natl Acad Sci U S A 1995;92:3439–43.
19. Jachetti E, Mazzoleni S, Grioni M, Ricupito A, Brambillasca C, Generoso L, et al. Prostate cancer stem cells are targets of both innate and adaptive immunity and elicit tumor-specific immune responses. Oncoimmunology 2013;2:e24520.
20. Garbers C, Spudy B, Aparicio-Siegmund S, Waetzig GH, Sommer J, Hölscher C, et al. An interleukin-6 receptor-dependent molecular switch mediates signal transduction of the IL-27 cytokine subunit p28 (IL30) via a gp130 protein receptor homodimer. J Biol Chem 2013;288:4346–54.
21. Ittmann M, Huang J, Radaelli E, Martin P, Signoretti S, Sullivan R, et al. Animal models of human prostate cancer: the consensus report of the New York meeting of the Mouse Models of Human Cancers Consortium Prostate Pathology Committee. Cancer Res 2013;73:2718–36.
22. Cheon H, Yang J, Stark GR. The functions of signal transducers and activators of transcriptions 1 and 3 as cytokine-inducible proteins. J Interferon Cytokine Res 2011;31:33–40.
23. Yu H, Pardoll D, Jove R. STATs in cancer inflammation and immunity: a leading role for STAT3. Nat Rev Cancer 2009;9:798–809.
24. Zlotnik A, Yoshie O. The chemokine superfamily revisited. Immunity 2012;36:705–16.
25. Weckermann D, Müller P, Wawroschek F, Harzmann R, Riethmüller G, Schlimok G. Disseminated cytokeratin positive tumor cells in the bone marrow of patients with prostate cancer: detection and prognostic value. J Urol 2001;166:699–703.
26. Legler DF, Loetscher M, Roos RS, Clark-Lewis I, Baggiolini M, Moser B. B cell-attracting chemokine 1, a human CXC chemokine expressed in lymphoid tissues, selectively attracts B lymphocytes via BLR1/CXCR5. J Exp Med 1998;187:655–60.
27. Dibra D, Cutrera J, Xia X, Kallakury B, Mishra L, Li S. Interleukin-30: a novel antiinflammatory cytokine candidate for prevention and treatment of inflammatory cytokine-induced liver injury. Hepatology 2012;55:1204–14.
28. Mitra A, Satelli A, Yan J, Xueqing X, Gagea M, Hunter CA, et al. IL30 (IL27p28) attenuates liver fibrosis through inducing NKG2D-rae1 interaction between NKT and activated hepatic stellate cells in mice. Hepatology 2014;60:2027–39.
29. Wang RX, Yu CR, Mahdi R, Egwuagu CE. Novel IL27p28/IL12p40 cytokine suppressed experimental autoimmune uveitis by inhibiting autoreactive Th1/Th17 cells and promoting expansion of regulatory T cells. J Biol Chem 2012;287:36012–21.
30. Weiss WA, Taylor SS, Shokat KM. Recognizing and exploiting differences between RNAi and small-molecule inhibitors. Nat Chem Biol 2007;3:739–44.
31. Godoy P, Cadenas C, Hellwig B, Marchan R, Stewart J, Reif R, et al. Interferon-inducible guanylate binding protein (GBP2) is associated with better prognosis in breast cancer and indicates an efficient T cell response. Breast Cancer 2014;21:491–9.
32. Iwai Y, Ishida M, Tanaka Y, Okazaki T, Honjo T, Minato N. Involvement of PD-L1 on tumor cells in the escape from host immune system and tumor immunotherapy by PD-L1 blockade. Proc Natl Acad Sci U S A 2002; 99:12293–7.
33. Pardoll DM. The blockade of immune checkpoints in cancer immunotherapy. Nat Rev Cancer 2012;12:252–64.
34. Merlo A, Casalini P, Carcangiu ML, Malventano C, Triulzi T, Mènard S, et al. FOXP3 expression and overall survival in breast cancer. J Clin Oncol 2009; 27:1746–52.
35. Hinz S, Pagerols-Raluy L, Oberg HH, Ammerpohl O, Grüssel S, Sipos B, et al. Foxp3 expression in pancreatic carcinoma cells as a novel mechanism of immune evasion in cancer. Cancer Res 2007;67:8344–50.
36. Kawai T, Akira S. The role of pattern-recognition receptors in innate immunity: update on Toll-like receptors. Nat Immunol 2010;11:373–84.
37. Sato Y, Goto Y, Narita N, Hoon DS. Cancer cells expressing toll-like receptors and the tumor microenvironment. Cancer Microenviron 2009;2 Suppl 1:205–14.
38. Rakoff-Nahoum S, Medzhitov R. Toll-like receptors and cancer. Nat Rev Cancer 2009;9:57–63.
39. Wang JQ, Jeelall YS, Ferguson LL, Horikawa K. Toll-like receptors and cancer: MYD88 mutation and inflammation. Front Immunol 2014; 5:367.
40. Matijevic Glavan T, Cipak Gasparovic A, Vérillaud B, Busson P, Pavelic J. Toll-like receptor 3 stimulation triggers metabolic reprogramming in pharyngeal cancer cell line through Myc, MAPK, and HIF. Mol Carcinog 2017;56:1214–26.
41. Goto Y, Arigami T, Kitago M, Nguyen SL, Narita N, Ferrone S, et al. Activation of Toll-like receptors 2, 3, and 4 on human melanoma cells induces inflammatory factors. Mol Cancer Ther 2008;7:3642–53.
42. Kuonen F, Laurent J, Secondini C, Lorusso G, Stehle JC, Rausch T, et al. Inhibition of the Kit ligand/c-Kit axis attenuates metastasis in a mouse model mimicking local breast cancer relapse after radiotherapy. Clin Cancer Res 2012;18:4365–74.
43. Balkwill F. Tumour necrosis factor and cancer. Nat Rev Cancer 2009; 9:361–71.
44. Gabrilovich DI, Ostrand-Rosenberg S, Bronte V. Coordinated regulation of myeloid cells by tumours. Nat Rev Immunol 2012;12:253–68.
45. Shtivelman E, Beer TM, Evans CP. Molecular pathways and targets in prostate cancer. Oncotarget 2014;5:7217–59.
46. Thoms JW, Dal Pra A, Anborgh PH, Christensen E, Fleshner N, Menard C, et al. Plasma osteopontin as a biomarker of prostate cancer aggression:

relationship to risk category and treatment response. Br J Cancer 2012; 107:840–6.
47. Koizumi K, Hojo S, Akashi T, Yasumoto K, Saiki I. Chemokine receptors in cancer metastasis and cancer cell-derived chemokines in host immune response. Cancer Sci 2007;98:1652–8.
48. Massagué J, Obenauf AC. Metastatic colonization by circulating tumour cells. Nature 2016;529:298–306.
49. Meijer J, Zeelenberg IS, Sipos B, Roos E. The CXCR5 chemokine receptor is expressed by carcinoma cells and promotes growth of colon carcinoma in the liver. Cancer Res 2006;66:9576–82.
50. Airoldi I, Cocco C, Morandi F, Prigione I, Pistoia V. CXCR5 may be involved in the attraction of human metastatic neuroblastoma cells to the bone marrow. Cancer Immunol Immunother 2008;57:541–8.
51. Pencik J, Schlederer M, Gruber W, Unger C, Walker SM, Chalaris A, et al. STAT3 regulated ARF expression suppresses prostate cancer metastasis. Nat Commun 2015;6:7736.
52. Canesin G, Evans-Axelsson S, Hellsten R, Sterner O, Krzyzanowska A, Andersson T, et al. The STAT3 inhibitor galiellalactone effectively reduces tumor growth and metastatic spread in an orthotopic xenograft mouse model of prostate cancer. Eur Urol 2016;69:400–4.
53. Don-Doncow N, Marginean F, Coleman I, Nelson PS, Ehrnström R, Krzyzanowska A, et al. Expression of STAT3 in prostate cancer metastases. Eur Urol 2017;71:313–6.
54. Gerlinger M, Catto JW, Orntoft TF, Real FX, Zwarthoff EC, Swanton C. Intratumour heterogeneity in urologic cancers: from molecular evidence to clinical implications. Eur Urol 2015;67:729–37.
55. Kroon P, Berry PA, Stower MJ, Rodrigues G, Mann VM, Simms M, et al. JAK-STAT blockade inhibits tumor initiation and clonogenic recovery of prostate cancer stem-like cells. Cancer Res 2013;73:5288–98.
56. Schroeder A, Herrmann A, Cherryholmes G, Kowolik C, Buettner R, Pal S, et al. Loss of androgen receptor expression promotes a stem-like cell phenotype in prostate cancer through STAT3 signaling. Cancer Res 2014; 74:1227–37.
57. Culig Z. STAT3 in prostate cancer: whom should we treat and when? Eur Urol 2017;71:317–8.
58. Fizazi K, De Bono JS, Flechon A, Heidenreich A, Voog E, Davis NB, et al. Randomised phase II study of siltuximab (CNTO 328), an anti-IL-6 monoclonal antibody, in combination with mitoxantrone/prednisone versus mitoxantrone/prednisone alone in metastatic castration-resistant prostate cancer. Eur J Cancer 2012;48:85–93.